Integrated manufacture of polymer and conductive tracks for real-world applications

Barbara Urasinska-Wojcik[a,*], Neil Chilton[b], Peter Todd[c], Christopher Elsworthy[c], Myles Bates[d], Gethin Roberts[d], Gregory J. Gibbons[a]

[a] *University of Warwick, Warwick Manufacturing Group, Coventry, CV4 7AL, United Kingdom*
[b] *Printed Electronics Limited, Tamworth, B77 5HH, United Kingdom*
[c] *C Enterprise (UK) Limited, Bristol, BS20 7AY, United Kingdom*
[d] *ITERATE Design + Innovation, Chepstow, NP16 5UH, United Kingdom*

* Corresponding author at: University of Warwick, Warwick Manufacturing Group, Coventry, CV4 7AL, United Kingdom. *E-mail address*: b.wojcik@warwick.ac.uk (B. Urasinska-Wojcik).

Keywords: Additive manufacturing, Conductive tracks, Hybrid 3D Printer, Integrated manufacture

ABSTRACT

The present study demonstrates for the first time a unique UK-designed and built Additive Manufacturing (AM) hybrid system that combines polymer based structural deposition with digital deposition of electrically conductive elements. This innovative manufacturing system is based on a multi-planar build approach to improve on many of the limitations associated with AM, such as poor surface finish, low geometric tolerance and poor robustness. Specifically, the approach involves a multi-planar Material Extrusion (ME) process in which separated build stations with up to 5 axes of motion replace traditional horizontally-sliced layer modelling. The construction of multi-material architectures also involved using multiple print systems in order to combine both ME and digital deposition of conductive material. To demonstrate multi-material 3D Printing (3DP) we used three thermoplastics to print specimens, on top of which a unique Ag nano-particulate ink was printed using a non-contact jetting process, during which drop characteristics such as shape, velocity, and volume were assessed using a bespoke drop watching system. Electrical analysis of printed conductive tracks on polymer surfaces was performed during mechanical testing (static tensile and flexural testing and dynamic fatigue testing) to assess robustness of the printed circuits. Both serpentine and straight line patterns were used in the testing of Ag particle loaded ink and they showed very similar resistance changes during mechanical exposure. Monitored resistance and stress changed as a function of strain exhibiting hysteresis with more prominent residual strain during stretching and compression cycles and 3-point bending flexural tests of PA and CoPA substrates. Bare and encapsulated tracks exhibited low electrical resistivity (1-3*10^{-6}Ω*m), and

its change was more rapid on ABS and minor on PA and CoPA when increasing tensile and flexural strain up to 1.2% and 0.8%, respectively. Resistance of Ag tracks on ABS also increased rapidly during fatigue testing and the tracks easily fractured during repeated stretching-compression cycles at 1% and 1.2% strain. No resistance changes of Ag tracks printed on PA and CoPA were observed at lower strain amplitudes whereas at higher strain amplitudes these changes were the lowest for conductive tracks on CoPA. Thermal analyses were conducted to determine the printed material's glass transition temperature (Tg), stability and degradation behavior to find the optimum annealing conditions post printing. The novel AM printer has the ability to fabricate fully functional objects in one build, including integrated printed circuitry and embedded electronics. It enables product designers and manufactures to produce functional saleable electronic products. This new technology also gives the opportunity for designers to improve existing products, as well as create new products with the added advantages of geometrically unconstrained 3DP.

1. Introduction

The recent increase in application of AM of products has resulted in new demands on AM system capability; and the ability to integrate both form and function within printed objects is the next frontier in the 3DP arena. AM is being explored in wide application areas including biomedical, automotive and aerospace; and fabrication of functional end-use products is currently a popular trend in this field [1]. To fabricate multi-functional 3D structures, various techniques such as ME [2], Vat Polymerisation (VP) – specifically Stereolithography (SL) [3], Digital Light Processing (DLP) [4] and Powder Bed Fusion (PBF) [5] are used to create single-material structures, but to incorporate multiple materials in the same build has been more challenging [6]. The ME process has made 3DP extremely affordable due to its simplicity and low implementation cost, and is therefore widely used as a product development, prototyping and manufacturing process [7]. Multi-functional 3D structures, such as those combining structural form with electronics, require the use of multiple technologies to address manufacturing challenges and improve functionality [8-10]. For example, Lopes et al. demonstrated the ability of the hybrid SL/Direct Wire (DW) technology for fabricating embedded electronic components [11]. Medina et al. introduced the combination of Direct Printing (DP) of conductive inks onto solid freeform fabricated structures [12,13]. Similar circuits and useful devices created by open-source fabrication systems have also been demonstrated by others [14-16]. In recent years, Stratasys Ltd and Optomec Inc reported the

use of Fused Deposition Modelling (FDM) with subsequent aerosol printing of conformal circuits [17-19]. A first commercial 3D printer combined with a pneumatic ink dispenser for creating conductive interconnects in 3D Printed structures has been introduced in 2015 by Lewis et al. and announced as a Voxel8 Developer's Kit 3D printer [20]. This affordable and highly useable printer is the first example of an economical desktop 3DP for electronics [21]. Since then many industry experts have intention to develop further innovative solutions for 3D Printed electronics; for example 3DP company Nano Dimension is currently leading the way in the field of 3D Printed circuit boards [22]. Also, research conducted at the University of Texas at El Paso (UTEP) has originally focused on manufacturing of 3D Printed electronic circuits and currently explores a multi-process AM called Multi^{3D} System [10]. The hybrid AM system developed by UTEP has the ability to perform subtractive manufacturing, wire embedding and pick and place processes, all while transferring a fabricated component with a robotic arm [9,23]. However, many of the conductive structures on dielectric substrates reported to date have been limited only to a single plane and the physical limitations of a thermal ME process have challenges reaching densities required for useful microelectronics [24]. To address some of these issues, Espalin et al. recently demonstrated a ME-based process that in a build sequence, provides a functional polymer substrate with sufficient density, and spatial features via thermal embedding technology with the targeted use of conductive inks [25]. Limitations of Espalin's approach were that the build was constrained to the planar XYZ geometries of the platform and the embedded discrete wires were unable to create sufficiently conductive surfaces required in, for example, ground planes of antennas or shielding planes in digital electronics [26]. In order to further expand the capabilities of 3DP, new functional inks, multi-nozzle print heads and printing platforms must be designed to print customised 3D electronic devices in a more scalable manner. Conductive inks have been used for over a decade in 3DP and can now be used to print conformal electronics with dense routing and improved resolution [27,28]. One characteristic of nanoparticle conductive inks for both aerosol spray and inkjet applications is that they only provide very thin layers (often less than one µm per printed layer), and in some cases require a relatively high temperature post-treatment to cure. This means that their performance is insufficient for high-power and high-frequency applications [26,28-30]. The much higher viscosity of screen printed inks (~5,000cP) over inkjet or aerosol inks (~10cP) permits screen-printed circuitry to be deposited at around ten µm, providing enhanced electrical conductivity, and has been used for many years in challenging applications.

To meet the requirements of future 3D Printed electronics that move beyond prototyping and into low volume production, we demonstrate a unique UK-designed and built 5-axis AM hybrid system ("IMPACT") with a large build volume that combines polymer based structural deposition with digital jet deposition of high viscosity electrically conductive ink with relatively low-temperature curing requirement. In this paper we address the challenges associated with dimensional accuracy, precision, repeatability and surface finish of ME parts, and thermal treatment of the conductive ink, and present data on the electrical performance of printed conductive tracks on various substrates whilst loaded under simulated real-world mechanical stresses.

2. Experimental

2.1. Additive Manufacturing Hybrid System

In this paper a novel hybrid AM system that combines a 5-axis ME 3D Printer (a mature method of depositing polymer filament) and a 4-axis non-contact jetting process for depositing thick conductive inks [31] (an advanced digital deposition system of high-performance conductive materials) is proposed. These technologies have not previously been combined, making this a truly innovative manufacturing system. A multi-planar build approach was employed to overcome many of the limitations of single plane manufacture, such as poor surface finish, poor geometric tolerance, lack of robustness, and the need for supporting structures. These two printing systems keep the 3D and 2D printing processes separate but share the same fixturing and positioning mechanics (Fig. 1a and 1b). The printer has a large cylindrical build volume of 700mm Φ x 500mm tall (Z). It has a 5-axis coordinate positioning system allowing deposition of material with a repeatable accuracy in the range of 20-50μm. This 5-axis capability ensures that the parts created have a much higher structural integrity than those created on a traditional 3-axis machine. The 5-axis rotation allows improved structural integrity of parts by manipulating direction of layers and removing the need for support structures. The machine is equipped with an automated tool change including subtractive spindle motor that enables the use of the dual ME head (with maximum nozzle temperature of 300°C) with direct drive extrusion feed and the piezoelectric print head sequentially (Fig. 1c). Our developed Computer-Aided Manufacturing (CAM) software drives the machine hardware in a safe and predictable way from a relatively simple machine path code.

(a)

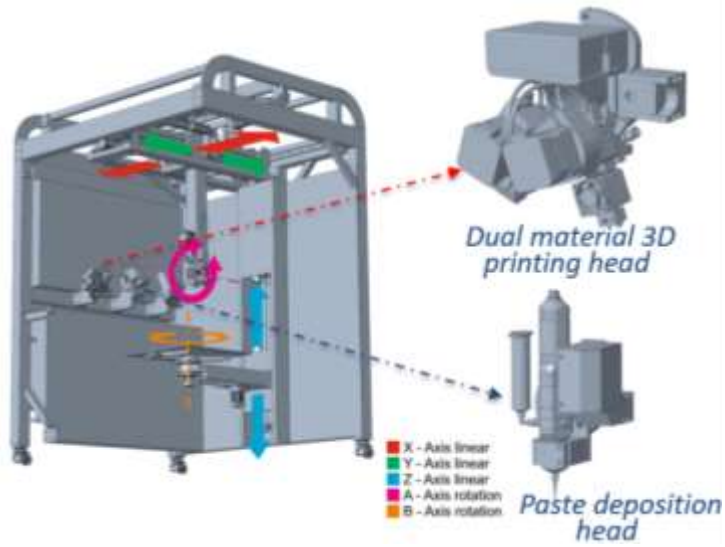

(b)

(c)

Fig. 1. Schematic illustration (a) and a photograph (b) of the additive manufacturing (AM) hybrid system. Photograph of the ME head that allows creation of spatial models on a 3D surface (c).

2.2. Sample Preparation

To demonstrate multi-material 3DP at CEL-UK (Portishead, UK), three thermoplastics acrylonitrile butadiene styrene (ABS), polyamide 6,6/6 copolymers (CoPA) and polyamide 12 (PA) with filament diameter 1.75±0.05mm were used to print specimens, on top of which the Ag-particulate ink with diameter around 100nm (Printed Electronics, Tamworth, UK) was printed in both straight and serpentine patterns, in a non-contact process, during which drop characteristics (shape, velocity, and volume) were assessed using a drop watching system. Fig. 2 presents a photograph of a single drop ejection of high viscosity conductive Ag nanoparticle paste travelling from the jetting head. Drop diameter is around 150μm in flight and forms a 300μm drop on the surface, and because the ink has high viscosity at high energy, these drops form elongated rods rather than a spherical surface.

Fig. 2. A photograph of a stroboscopic droplet ejection of a single drop of high viscosity conductive Ag paste travelling from the piezo-and-pressure-driven head.

After printing Ag conductive patterns, samples were air annealed in an oven at 80°C for 1h. The diameter of the ME nozzle was 0.4mm and the extrusion temperature was set at 235, 250 and 230°C for ABS, CoPA and PA filaments respectively. The temperature of the build bed was set at 80, 70 and 120°C for ABS, CoPA and PA respectively. A layer thickness of 0.2mm was used for all thermoplastic materials. The diameter of the jetting nozzle was 50µm. Specimens for tensile, 3-point bend and fatigue testing (at least three of each type) were printed with 40% infill density with consecutive layers of diagonal deposition. Conductive tracks were also partially encapsulated with a top 1mm printed layer of the same thermoplastic material as used for the base substrate.

2.3. Mechanical and Electrical Testing

Static tensile and 3-point bend testing of samples was performed using an Instron 5800R (Instron, High Wycomb, UK) universal testing machine with a non-contacting video extensometer for real-time, high-accuracy strain measurements (Fig. 3a). Fatigue tests were performed using an Instron 8872 (Instron, High Wycomb, UK) servo-hydraulic fatigue testing system (25kN). Specimens were designed in accordance with the ASTM D638 Type 1 Standard for the tensile and fatigue tests and ASTM D7264 M07 Procedure A Standard for 3-point bend test (Fig. 3b). Dog-bone specimens 170x20x4mm were used for tensile and fatigue tests and were identical for both test regimes. Beam shape specimens 80x10x4mm were used for 3-point bend tests during which tensile stress was produced in the convex side of specimens (surface containing the conductive tracks), and compressive stress was produced in the concave side. Load-deflection data up to 5mm of deflection for PA and CoPA and 2mm for ABS were recorded. The span was 76mm for all loadings. Electrical

contact with the Ag-based conductive tracks were made using a four-terminal measurement lead set connected to BS407 micro ohmmeter (Aim and Thurlby Thandar Instruments, Huntingdon, UK) for accurate measurement of low resistance (Fig. 3c and 3d). Electrical resistivity was then calculated using Equation 1:

$$\rho = R\frac{A}{l} \qquad \text{Equation 1}$$

where ρ is electrical resistivity in Ω·m, R is resistance in Ω, A is a cross-sectional area in m^2 and l is the length in m.

The vertical length between the electrical contacts was maintained constant for samples of the same type. For tensile and fatigue tests the overall length of printed track was 90mm (straight) and 150mm (serpentine) respectively; for 3-point bend tests the overall length was 3.95mm (straight) and 6.2mm (serpentine) respectively. The print width of straight and serpentine tracks was 2.2mm and 1.2mm, respectively (Fig. 3). Dimensions of each specimen were measured before subjecting to mechanical tests. Variations of the printed samples were as follows: (i) PA: width ± 0.05mm; thickness ± 0.02mm; (ii) ABS: width ± 0.06mm; thickness ± 0.06mm; (iii) CoPA: width ± 0.04mm; thickness ± 0.08mm.

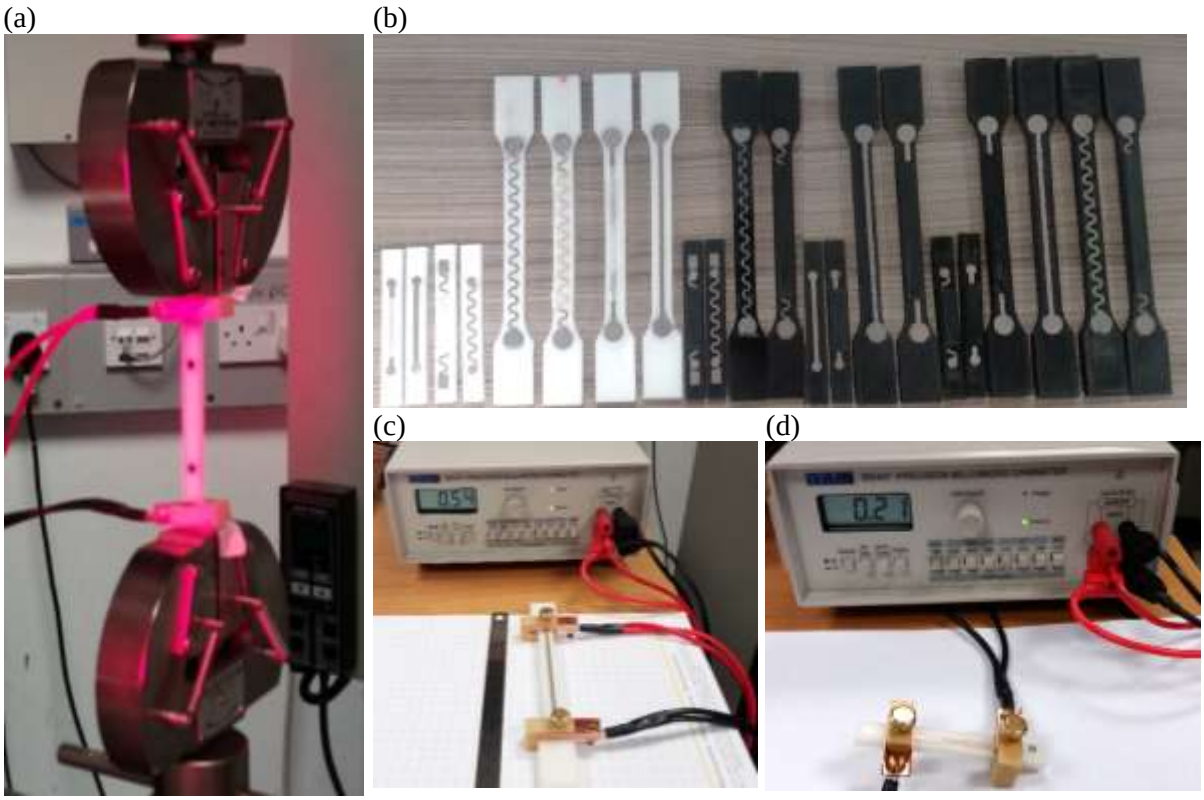

Fig. 3. Instron 5800R tensile test machine with a specimen clamped (a). Image of PA, CoPA and ABS substrates with bare and partially encapsulated printed tracks (b). PA with Ag-based track specimen for tensile (c) and 3-point bend (d) testing connected to the ohmmeter.

In static tensile and flexural tests, specimens were subjected to increasing and reducing strain during each loading-unloading cycle in which the electrical resistance of the printed tracks was monitored and stress vs. strain and resistance vs. strain characteristics were documented for each test. A series of fatigue tests were performed to evaluate degradation of conductive tracks on thermoplastic substrates. During fatigue tests, specimens were subjected to 100 repeated cycles at strain amplitude 0.25%, 0.5%, 1% and 1.2% and strain rate of $0.1s^{-1}$. The resistance of printed tracks was monitored in the linear region of their stress-strain characteristics.

2.4. Surface Studies of Conductive Patterns

Surface characterisation of Ag conductive patterns was performed using a Contour GT-X optical profilometer (Bruker UK, Coventry, UK).

2.5. Thermal Analyses

Thermogravimetric analysis (TGA) was performed using a TGA 1 thermal analyser (Mettler-Toledo Ltd, Leicester, UK). Samples of thermoplastic material of initial weight 5-7mg were placed in an Al_2O_3 crucible and scans were performed at over a temperature range of 25 to 600°C under air atmosphere with a heating rate of 10°C min^{-1}.

Differential scanning calorimetry (DSC) analysis was performed using a DSC 1 calorimeter (Mettler-Toledo Ltd, Leicester, UK). Samples of each thermoplastic material (5-6.5mg) were placed in aluminium pans. The scans were performed over a temperature range of 25 to 200°C or 250°C in a nitrogen atmosphere with a heating rate of 10°C min^{-1}.

Dynamic mechanical thermal analysis (DMTA) was carried out with a Triton Tritec dynamic mechanical thermal analyser (Triton Technology Ltd, Keyworth, UK) equipped with a single cantilever clamp. 3D Printed specimens of rectangular shape (5x10x0.5mm) were used for testing. Dynamic storage modulus and tanδ were recorded from 24 to 160°C for PA and CoPA, and from 24 to 120°C for ABS at a heating rate of 2°C min^{-1}, with a controlled sinusoidal strain with a fixed frequency of 1Hz.

3. Results and Discussion

3.1. 3D Printed Thermoplastic Materials Characterisation by Thermal Analysis

Thermal analyses were performed to determine the printed material's glass transition temperature, stability and degradation behavior to find the optimum ink annealing conditions post-printing. Results obtained by DSC, TGA and DMTA are reported in Table 1, 2 and 3, respectively. From the TGA curves the mass decrement during heating was determined; whereas the temperature of the maximum rate of the process and initial decomposition temperatures were determined from the temperature derivative curves.

T_g was evaluated from the DMTA analyses as temperature values corresponding to the tanδ peak. The results from thermal analysis of the 3D Printed thermoplastics were helpful in material selection and criteria development to guide deposition parameters of conductive material on the thermoplastic polymers. The initial cure temperature of 80°C for Ag ink was above the T_g of PA and CoPA. This could cause the properties to change within the polymer substrates and this could also have an effect on the ink adhesion. The thermal impact on the substrates when processing the Ag ink was minimized by reducing the cure temperature to 40°C and increasing the cure duration from 60min to 180min. Localized processing techniques such as laser heating could also be implemented thereby minimizing the heat input into the substrates.

Table 1
DSC results of 3D Printed thermoplastic materials.

Material	T_g [°C]	Melting Temperature [°C]	Crystallization Temperature [°C]
PA	47 ± 2	178 ± 1	153 ± 2
CoPA	79 ± 4	188 ± 2	145 ± 1
ABS	99 ± 6	Amorphous	Amorphous

Table 2
Results from TGA analysis of 3D Printed thermoplastic materials. IDT: initial decomposition temperature; $D_{0.1}$: temperature for 10wt% decomposition; $D_{1/2}$: temperature for 50wt% decomposition; MRDT: temperature for the maximum rate of decomposition.

Material	IDT [°C]	$D_{0.1}$ [°C]	$D_{1/2}$ [°C]	MRDT [°C]	Residue [%]
PA	387.4 ± 0.8	404.9 ± 0.1	457.2 ± 0.2	462.5 ± 2.1	0.1 ± 0.1
CoPA	332.8 ± 0.4	371.6 ± 1.3	427.2 ± 0.2	426.3 ± 0.5	2.5 ± 0.1
ABS	288.5 ± 0.7	362.4 ± 0.1	410.8 ± 0.4	406.3 ± 0.4	4.5 ± 0.1

Table 3
Results from DMTA analysis of 3D Printed thermoplastic materials.

Material	T_g [^oC]	Storage Modulus @ RT [MPa]
PA	52 ± 2	1140 ± 70
CoPA	56 ± 2	911 ± 50
ABS	92 ± 1	757 ± 150

3.2. Surface Characterisation of Ag Conductive Patterns

Thickness of conductive tracks varied between 75 and 90µm. The average roughness (Ra) values of the conductive surface area of 0.9x1.3mm on PA, CoPA and ABS were 22±1, 21±1 and 23±3µm, respectively. The similar values of Ra suggest that the Ag nanoparticles had a uniform distribution and higher chance to sinter together, thus presenting high conductivity.

3.3 Mechanical and Electrical Characterisation of 3D Printed Thermoplastic Materials Integrated with Conductive Tracks

Electrical analysis of printed conductive tracks on polymer surfaces during mechanical testing (static tensile and flexural testing and fatigue testing) were performed to assess robustness of the electrical circuits. Both bare and partially encapsulated serpentine and straight line patterns were used in the testing of Ag particle-loaded ink printed on thermoplastic substrates to assess the effect of track encapsulation on electrical performance of the track during mechanical loading. PA, CoPA and ABS samples integrated with Ag conductive tracks were loaded to three different maximum strains of 1.6, 1.8 and 1.2%, respectively, and these values corresponded to the proportional limit of each material.

Mechanical stress and electrical resistance changed as a function of strain exhibiting hysteresis during stretching and compression cycles and bending-release cycles (Fig. 4 and Fig. 5). Particularly, the unloading paths show more prominent hysteresis loops with a residual strain in the case of PA and CoPA (Table 4).

Table 4
Average residual strain values recorded during mechanical testing of 3D Printed thermoplastic substrates.

	Residual strain [%] – unencapsulated samples			**Residual strain [%] – encapsulated samples**		
	PA	**CoPA**	**ABS**	**PA**	**CoPA**	**ABS**
Tensile tests	0.12 ± 0.02	0.33 ± 0.04	0.04 ± 0.03	0.19 ± 0.04	0.37 ± 0.11	0.03 ± 0.02
Flexural tests	0.25 ± 0.07	0.27 ± 0.09	0.04 ± 0.02	0.26 ± 0.09	0.38 ± 0.13	0.05 ± 0.01

Bare tracks prior to loading exhibited in most cases low electrical resistance (0.5-1.5Ω; 1-3*10^{-6}Ω*m for tensile tests and 0.1-0.5Ω; 0.1-2*10^{-6}Ω*m for 3-point bend tests) and its change was more rapid on CoPA and ABS and negligible with almost no hysteresis on PA when increasing tensile or flexural strain. These resistivity values are two orders of magnitude higher compared to bulk resistivity of copper at 1.68*10^{-8}Ω*m, traditionally used for printed circuit boards (PCBs). Average values of at least three specimens of each sample type are reported in Tables 5-10. A small variation of thickness of the conductive ink tracks does not have any significant effect on resistance. Lower resistivity values of tracks printed on PA and ABS subjected to tensile and bend tests are likely due to densification of the conductive ink track and the increased contact area between the individual nanoparticles. Both ABS and CoPA substrates required higher stress to stretch or deflect the same distance than PA which has much lower modulus of elasticity (tensile modulus: 640±30MPa; flexural modulus: 964±22MPa) compared to the former two. For comparison, tensile and flexural modulus values are 863±45MPa and 1280±20MPa for ABS and 806±50MPa and 1916±1MPa for CoPA, respectively. This explains the higher stiffness of both ABS and CoPA substrates.

Partially encapsulated samples exposed to tensile and bend tests required slightly higher stress to stretch or deflect the same distance compared to unencapsulated samples, and elongation of ABS encapsulated specimens to 1.2% tensile strain led to crack growth and specimen fracture. Resistivity of encapsulated Ag tracks on PA exposed to stretching and bending was similar to the values obtained for bare tracks, whereas in the case of ABS these values were three times higher at 0.5% tensile strain (not shown in tables) and remained unchanged during 3-point bend tests. Low flexural stress slightly decreased electrical resistivity of encapsulated Ag tracks on CoPA compared to the bare tracks.

(a)

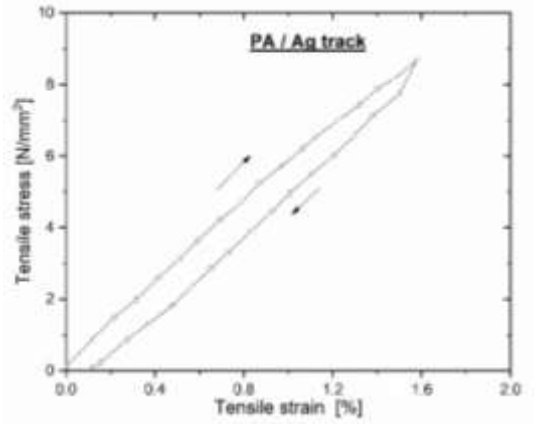

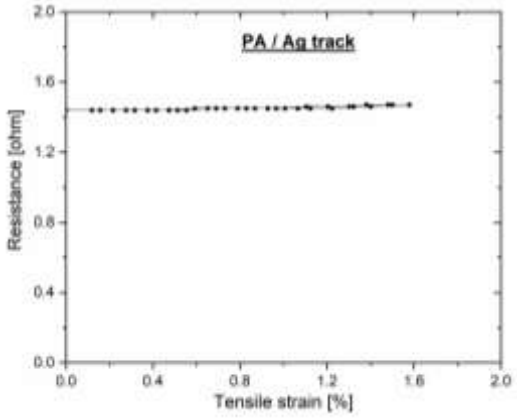

(b)

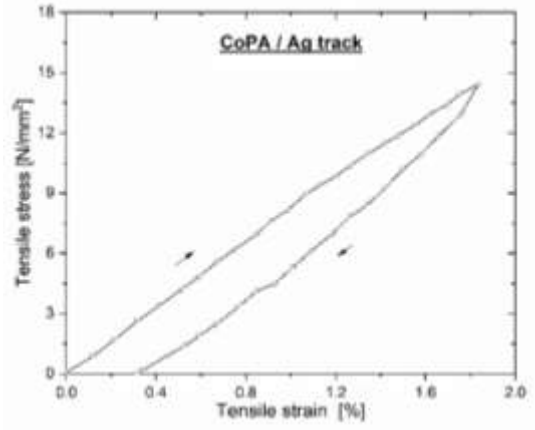

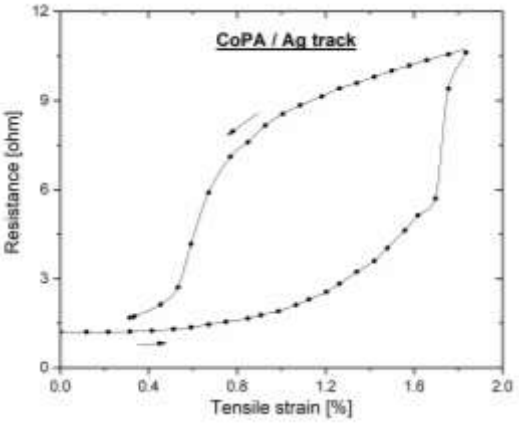

(c)

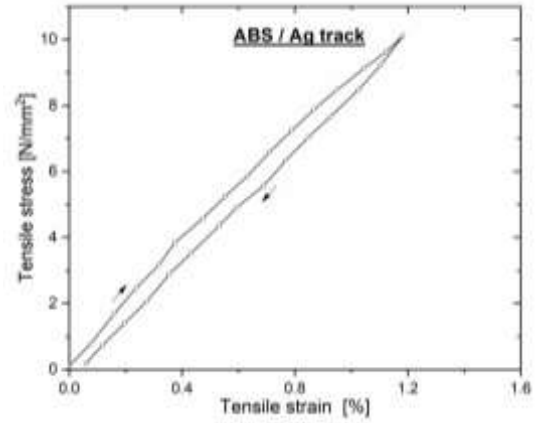

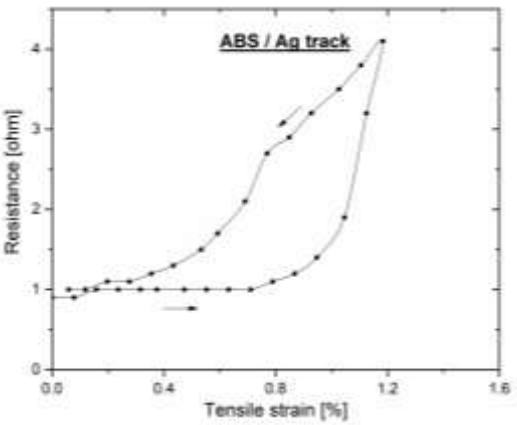

Fig. 4. Typical tensile test results showing stress-strain and resistance-strain characteristics of PA (a), CoPA (b) and ABS (c) substrates with conductive tracks printed on top in serpentine pattern.

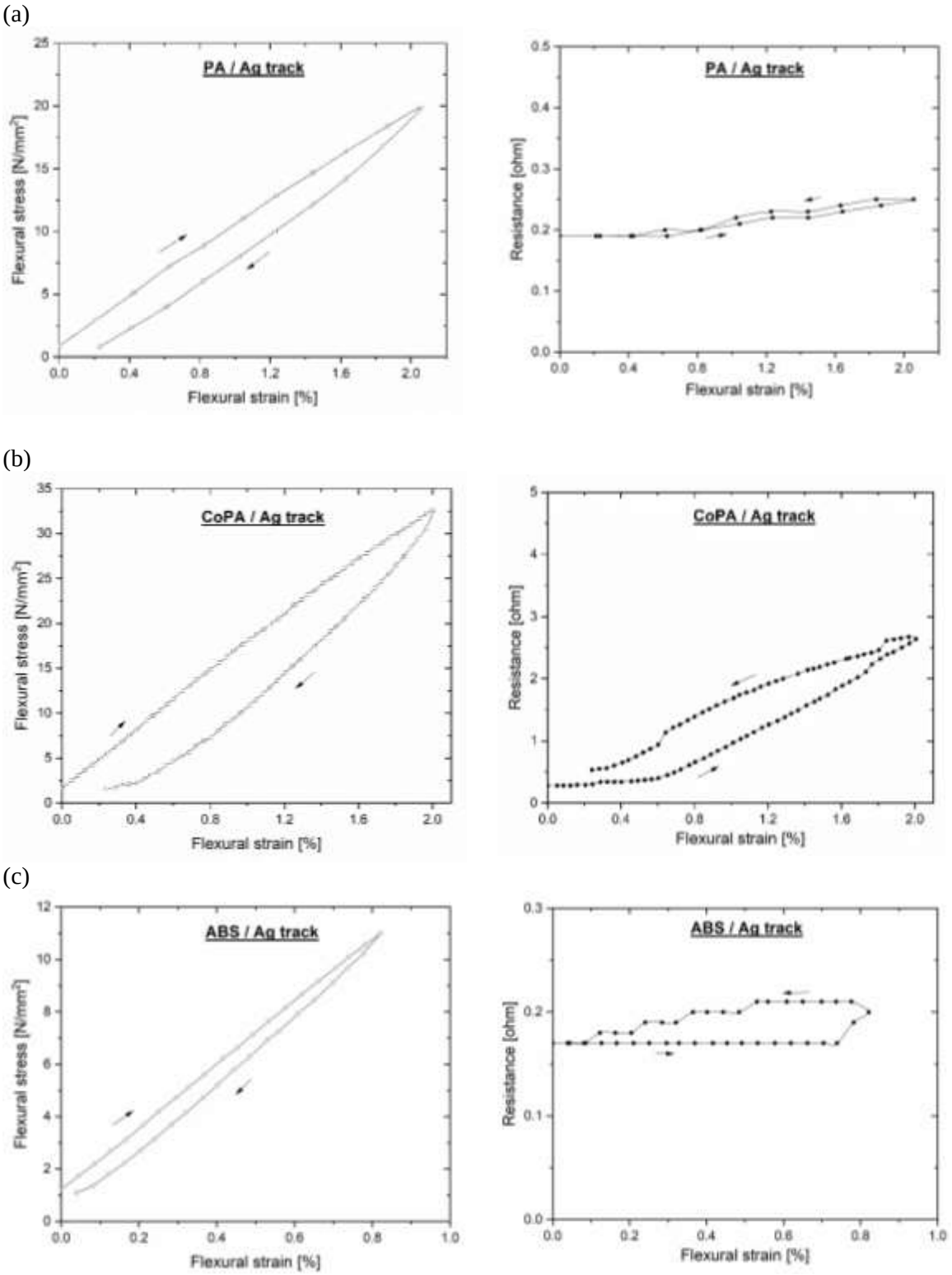

Fig. 5. Typical 3-point bend test results showing stress-strain and resistance-strain characteristics of PA (a), CoPA (b) and ABS (c) substrates with conductive tracks printed on top in straight pattern.

Table 5
Average tensile test results of Ag tracks printed on PA substrates.

PA/Ag & PA/Ag/PA	**Average tensile stress [MPa] @ 1.2% strain**	**Resistance increase [%] @ 1.2% strain**	**Average electrical resistivity * 10^{-6} [Ω*m] @ 1.2% strain**
Bare Ag track - straight	5.9 ± 0.1	101 ± 1	1.1 ± 0.1
Bare Ag track - serpentine	6.9 ± 0.1	101 ± 1	1.1 ± 0.4
Encapsulated Ag track - straight	6.5 ± 0.7	141 ± 41	1.5 ± 0.6
Encapsulated Ag track - serpentine	7.5 ± 0.7	120 ± 20	3 ± 1

Table 6
Average tensile test results of Ag tracks printed on CoPA substrates.

CoPA/Ag & CoPA/Ag/CoPA	**Average tensile stress [MPa] @ 1.2% strain**	**Resistance increase [%] @ 1.2% strain**	**Average electrical resistivity * 10^{-6} [Ω*m] @ 1.2% strain**
Bare Ag track - straight	10 ± 2	151 ± 31	3.0 ± 0.2
Bare Ag track - serpentine	11 ± 1	105 ± 6	2.9 ± 0.3
Encapsulated Ag track - straight	10.7 ± 0.2	185 ± 13	6 ± 2
Encapsulated Ag track - serpentine	12 ± 1	228 ± 23	6.7 ± 0.7

Table 7
Average tensile test results of Ag tracks printed on ABS substrates.

ABS/Ag	**Average tensile stress [MPa] @ 1.2% strain**	**Resistance increase [%] @ 1.2% strain**	**Average electrical resistivity * 10^{-6} [Ω*m] @ 1.2% strain**
Bare Ag track - straight	9.1 ± 0.3	159 ± 39	2.4 ± 1.2
Bare Ag track - serpentine	9.9 ± 0.2	364 ± 129	1.9 ± 0.4

Table 8
Average 3-point bend test results of Ag tracks printed on PA substrates.

PA/Ag & PA/Ag/PA	**Average flexural stress [MPa] @ 0.8% strain**	**Resistance increase [%] @ 0.8% strain**	**Average electrical resistivity * 10^{-6} [Ω*m] @ 0.8% strain**
Bare Ag track - straight	8.7 ± 0.2	103 ± 3	1.0 ± 0.2
Bare Ag track - serpentine	11.1 ± 0.8	106 ± 8	1.0 ± 0.6
Encapsulated Ag track - straight	12 ± 2	104 ± 7	0.9 ± 0.3
Encapsulated Ag track - serpentine	16 ± 2	110 ± 5	1.2 ± 0.5

Table 9
Average 3-point bend test results of Ag tracks printed on CoPA substrates.

CoPA/Ag & CoPA/Ag/CoPA	**Average flexural stress [MPa] @ 0.8% strain**	**Resistance increase [%] @ 0.8% strain**	**Average electrical resistivity * 10^{-6} [Ω*m] @ 0.8% strain**
Bare Ag track - straight	15.4 ± 0.8	115 ± 5	0.7 ± 0.1
Bare Ag track - serpentine	16.9 ± 0.8	114 ± 9	1.8 ± 0.2
Encapsulated Ag track - straight	21 ± 2	111 ± 4	0.7 ± 0.1
Encapsulated Ag track - serpentine	20.1 ± 0.4	112 ± 12	0.9 ± 0.2

Table 10
Average 3-point bend test results of Ag tracks printed on ABS substrates.

ABS/Ag & ABS/Ag/ABS	**Average flexural stress [MPa] @ 0.8% strain**	**Resistance increase [%] @ 0.8% strain**	**Average electrical resistivity * 10^{-6} [Ω*m] @ 0.8% strain**
Bare Ag track - straight	12 ± 1	124 ± 9	1.2 ± 0.2
Bare Ag track - serpentine	12.7 ± 0.1	105 ± 1	2.7 ± 0.1
Encapsulated Ag track - straight	15 ± 13	113 ± 7	2.2 ± 0.5
Encapsulated Ag track - serpentine	17 ± 2	109 ± 4	2.2 ± 0.9

Degradation of deposited Ag ink properties on PA, CoPA and ABS was assessed by performing a series of fatigue tests. These cyclic loading tests were conducted under fully reversed total strain amplitude control in air. The strain amplitude varied from 0.25% to 1.2%, and the strain rate was $0.1s^{-1}$. Cyclic stress response curves showing the relationship between the stress amplitude and the number of cycles at four different total strain amplitudes are shown in Fig. 6-8. All experiments were carried out on individual specimens. Both types of printed patterns on PA, ABS and CoPA showed very similar resistance changes during mechanical exposure.

Resistance of serpentine Ag tracks on PA remained still unchanged across hundreds of repeated cycles at strain amplitude 0.25 and 0.5% (Fig. 6a-b), and was 4 and 12 times higher after 100 fatigue cycles at strain amplitude 1 and 1.2% (Fig. 6c-d). Resistance of conductive serpentine patters printed on ABS changed negligibly across hundreds of repeated cycles at strain amplitude 0.25% (Fig. 7a), but increased 2.5 times after a 100 fatigue cycles at strain amplitude 0.5% (Fig. 7b). Several large cracks were observed in the stretched metal conductive tracks on ABS substrates during fatigue testing at 1% and 1.2% strain amplitude and the optical microscopy images of a track before and after the experiment are presented in Fig. 9. The cracks propagated along the track width direction, which was nearly perpendicular to the stretching direction. In this case, the tracks lost its conductivity as shown in Fig. 7c-d. Resistance of Ag tracks on CoPA remained unchanged across hundreds of repeated cycles at strain amplitude 0.25% (Fig. 8a), and was up to 1.5 times higher after 100 fatigue cycles at strain amplitude 0.5% (Fig. 8b). For strain amplitude 1% and 1.2%, resistance change was 2 and 3 times higher respectively after the end of dynamic testing (Fig. 8c-d). Typical stress and resistance values of PA, ABS and CoPA substrates integrated with Ag tracks subjected to fatigue tests at 0.25, 0.5, 1 and 1.2% strain are included in Tables 11-14.

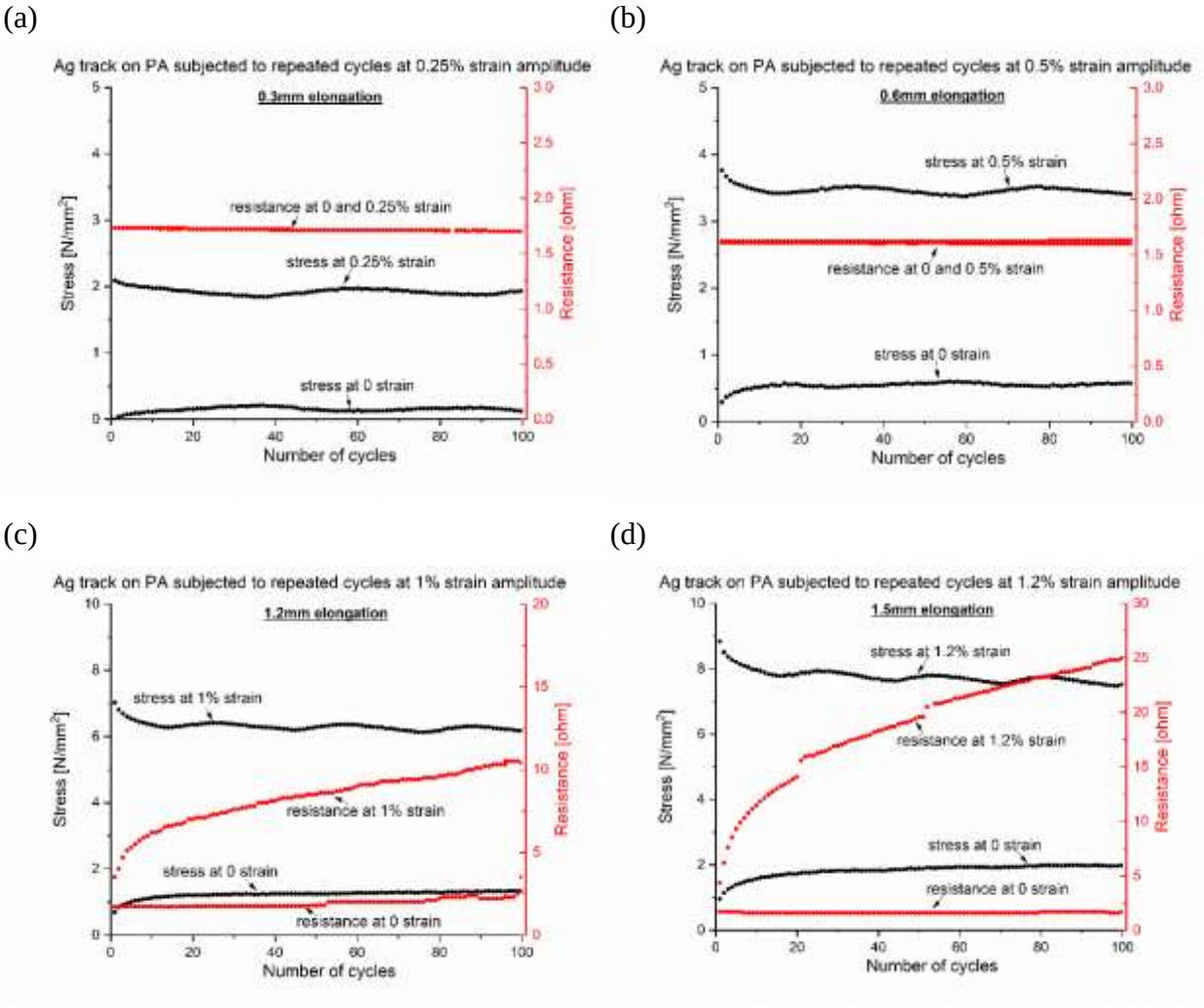

Fig. 6. Typical results from fatigue tensile tests performed on bare Ag tracks printed on PA substrates.

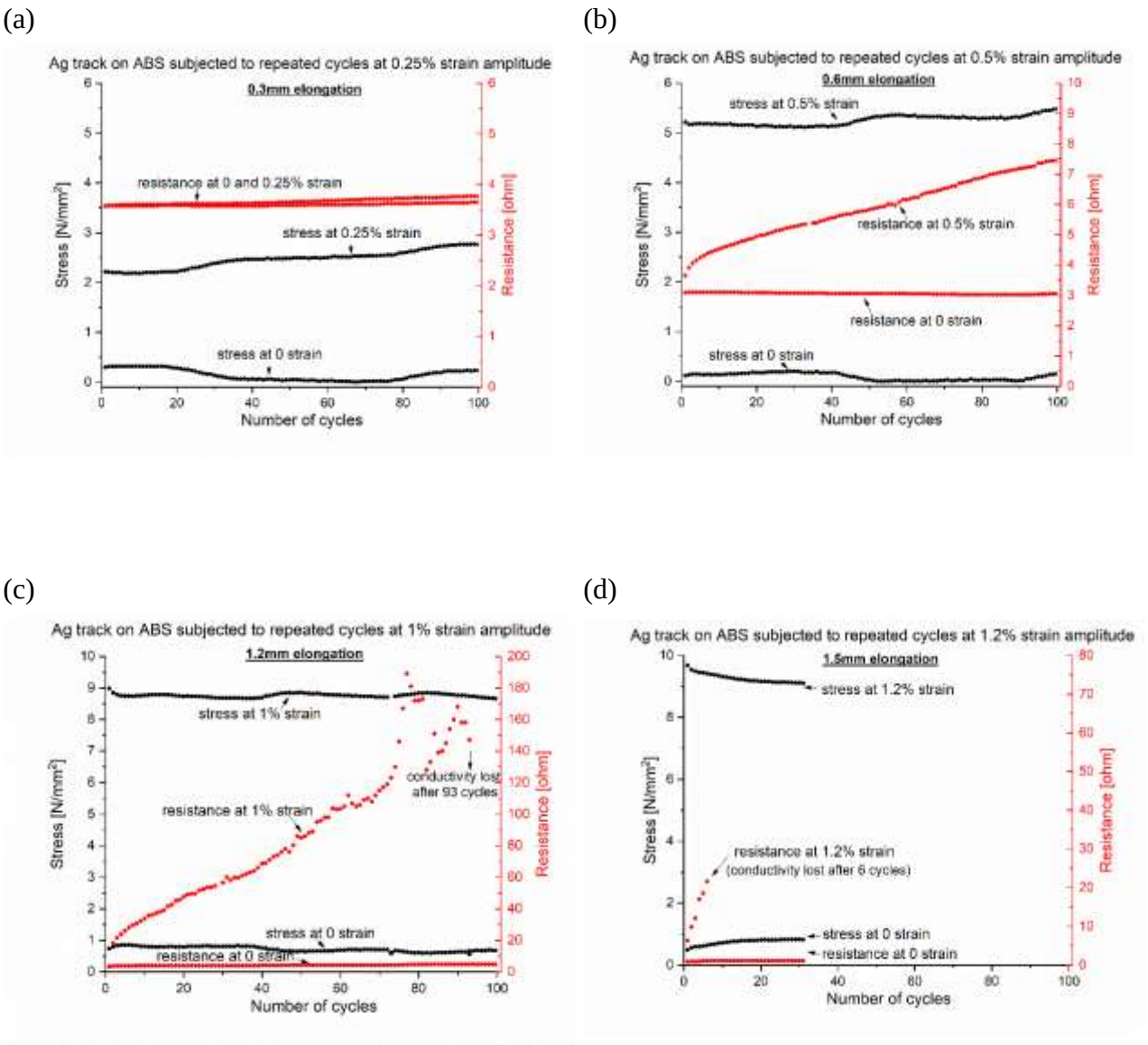

Fig. 7. Typical results from fatigue tensile tests performed on bare Ag tracks printed on ABS substrates.

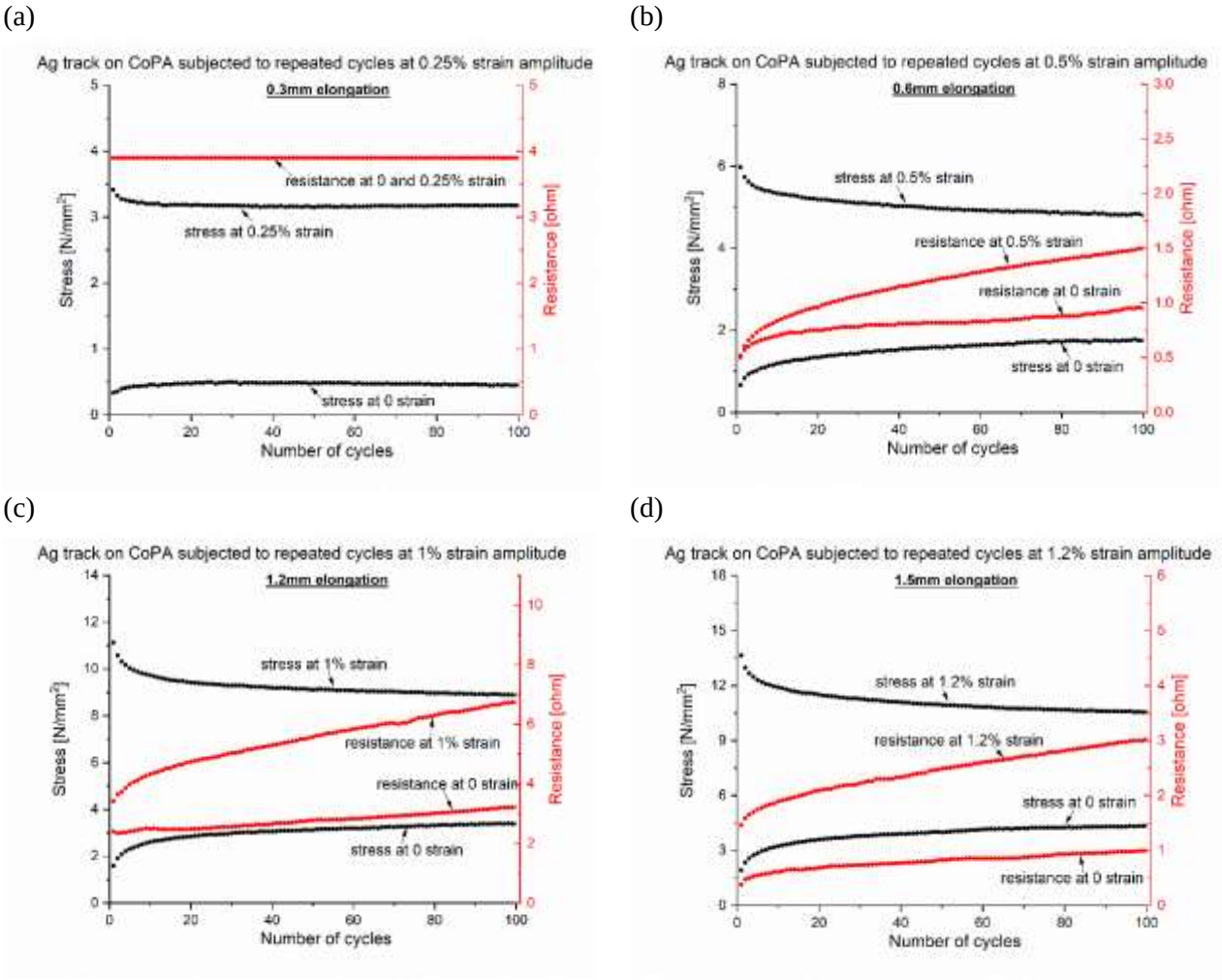

Fig. 8. Typical results from fatigue tensile tests performed on bare Ag tracks printed on CoPA substrates.

Table 11
Typical stress and resistance values of PA, ABS and CoPA with Ag tracks at 0.25% strain.

	Stress [MPa] @ 1st cycle	Resistance [Ω] @ 1st cycle	Stress [MPa] @ 100th cycle	Resistance [Ω] @ 100th cycle	Δ Stress [MPa]	Δ Resistance [Ω]
Ag/PA	2.1	1.7	1.9	1.7	0.2	0
Ag/ABS	2.2	3.6	2.7	3.8	0.5	0.2
Ag/CoPA	3.4	3.9	3.2	3.9	0.2	0

Table 12
Typical stress and resistance values of PA, ABS and CoPA with Ag tracks at 0.5% strain.

	Stress [MPa] @ 1st cycle	Resistance [Ω] @ 1st cycle	Stress [MPa] @ 100th cycle	Resistance [Ω] @ 100th cycle	Δ Stress [MPa]	Δ Resistance [Ω]
Ag/PA	3.8	1.6	3.4	1.6	0.4	0
Ag/ABS	5.2	3.7	5.5	7.4	0.3	3.7
Ag/CoPA	7.9	4.6	6.9	5.5	1.0	0.9

Table 13
Typical stress and resistance values of PA, ABS and CoPA with Ag tracks at 1% strain.

	Stress [MPa] @ 1st cycle	Resistance [Ω] @ 1st cycle	Stress [MPa] @ 100th cycle	Resistance [Ω] @ 100th cycle	Δ Stress [MPa]	Δ Resistance [Ω]
Ag/PA	7.0	4.4	6.2	25	0.8	20.6
Ag/ABS	9.0	3.6	8.7	-	0.3	-
Ag/CoPA	11.1	6.7	8.9	8.9	2.2	2.2

Table 14
Typical stress and resistance values of PA, ABS and CoPA with Ag tracks at 1.2% strain.

	Stress [MPa] @ 1st cycle	Resistance [Ω] @ 1st cycle	Stress [MPa] @ 100th cycle	Resistance [Ω] @ 100th cycle	Δ Stress [MPa]	Δ Resistance [Ω]
Ag/PA	8.8	4.4	7.5	25	1.3	19
Ag/ABS	9.7	6.4	-	-	-	-
Ag/CoPA	13.6	1.5	10.6	3.0	3	1.5

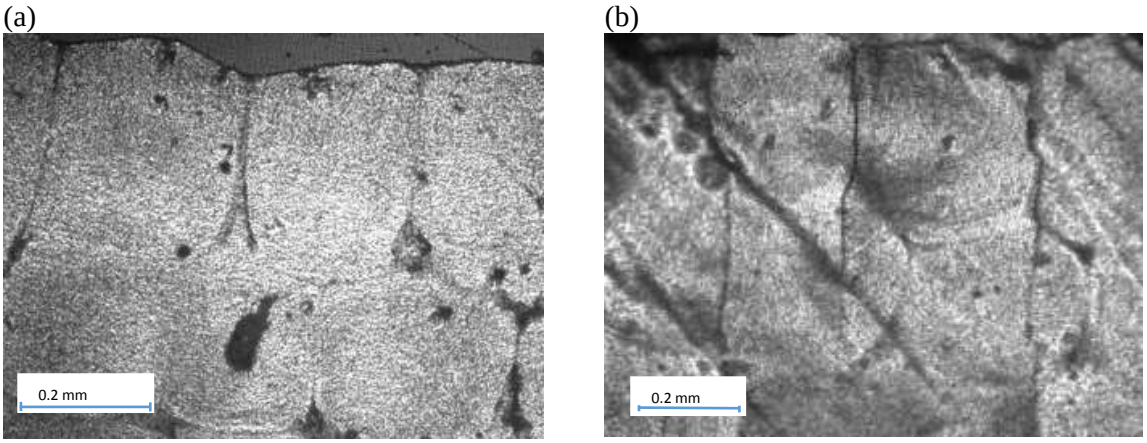

Fig. 9. Optical microscopy images of a Ag track on ABS before (a) and after (b) fatigue testing at 1% strain amplitude.

4. Conclusions

A hybrid system that combines polymer based structural deposition with digital deposition of electrically conductive elements was successfully developed. This hybrid Additive Manufacturing machine has the ability to fabricate fully functional objects with embedded electrical circuitry in one build reducing at the same time, the need for post assembly and finishing processes. The system has capabilities of Material Extrusion in 5 axes with high surface finish with minimal porosity of ME parts and advanced digital deposition in 4 axes of

a high-performance conductive material with low-temperature curing. This will enable parts to be built with a greater degree of geometric freedom and a higher level of structural integrity.

We demonstrated the fundamental capabilities provided by this multi-functional system through the fabrication and characterisation of printed conductive tracks on polymer surfaces. Conductivity of the printed tracks could be further improved by implementation of a laser system for *in situ* curing of Ag-based inks prior to continuing additional fabrication steps. In this work we demonstrated that these highly conductive tracks in both linear and serpentine patterns can now be seamlessly integrated into dielectric substrates, and therefore minimise or eliminate the need for wires, offering significant weight reductions of printed products. The following conclusions can be made to identify the best material for project related requirements.

1. PA has the ability to withstand significant mechanical stress (it has lower modulus of elasticity compared to ABS and CoPA). It is suitable for 3DP tools, functional prototypes and end-use parts. Ag tracks deposited on PA show low resistivity values, therefore PA is the most appropriate material for internal circuits which are higher voltage and can also be used to protect tracks from damage due to the small resistance changes observed.
2. CoPA is a versatile choice for creating consistently smooth and detailed prints, and can also be used as an insulator for protection of the conductive tracks. Resistance changes of Ag tracks printed on CoPA were the lowest particularly at higher strain amplitudes during fatigue testing. The material has a high stiffness, similar to ABS, and requires a high stress to deform.
3. ABS requires similar levels of stress as CoPA during stretching but slightly lower stress during bending. Resistance of Ag tracks on ABS increased rapidly during fatigue and tensile testing and the tracks easily fractured during repeated stretching-compression cycles at 1% and 1.2% strain amplitude.

Two conductive patterns were used and these designs may be crucial when dealing with more flexible substrates. Serpentine patterns were used to add length to tracks and they occupy more surface area than straight lines. Resistance changes of serpentine tracks were slightly higher compared to changes observed in straight tracks.

The proposed new technology that joins polymer deposition and digital deposition of electrically conductive elements, provides a chance for designers to improve existing

products as well as create new products. Examples of this include minimal assembly of bionic prostheses with incorporated electronics, embedded antennas/Near-Field Communication (NFC) systems, surface fracture identification with conductive tracks, and the production of forms that had previously not been possible without the use of support material. Printing flexible or strong parts can now be easy and intuitive.

Apart from implementation of the *in situ* curing system, our next plan is also to incorporate an automated pick and place system to surface mount electronic components within an integrated AM structure. The components will then be interconnected via printed conductive traces, thus eliminating the need for copper wires. The machine has the capability to create fully functional electro-mechanical products straight off the machine bed. The work presented in this paper shows 2D conductive printing but 2.5D and even more complex shapes such as drawing a spline on a 3D surface are within the capability of the machine and the simple control software. We are currently developing a new Computer-Aided Design (CAD)/CAM software and designing new tools which will: (*i*) enable the full 5-axis capability of the machine to be accessible to designers early in design phases, (*ii*) allow automated creation of more complex objects, (*iii*) provide simulation to prevent mistakes and find new use cases through virtual experimentation and (*iv*) include analysis tools to encourage digital integration in conservative areas of manufacturing. All the above features will make the machine more valuable. The improved hybrid system will help to reduce weight and assembly time, and create geometries that are currently impossible to build.

Acknowledgments

This work was supported by the UK Research and Innovation Project Grant: 103463 (IMPACT - Integrated Manufacture of Polymers and Conductive Tracks). Authors would like to thank Dr Nadia Kourra for the support on crack analysis in conductive tracks.

References

[1] Y. Xu, X. Wu, X. Guo, B. Kong, M. Zhang, X. Qian, S. Mi, W. Su, The Boom in 3D-Printed Sensor Technology, Sensors, 17 (2017) 1166.

[2] S.H. Masood, Intelligent rapid prototyping with fused deposition modelling, Rapid Prototyp. J. 2 (1996) 24-33.

[3] M.N. Cooke, D. Fisher, D. Dean, C. Rimnac, A.G. Mikos, Use of stereolithography to manufacture critical-sized 3D biodegradable scaffolds for bone ingrowth, J. Biomed. Mater. Res. Part B, 64B (2003) 65-69.

[4] I. Cooperstein, M. Layani, S. Magdassi, 3D printing of porous structures by UV-curable O/W emulsion for fabrication of conductive objects, J. Mater. Chem. C, 3 (2015) 2040-2044.

[5] M. Agarwala, D. Bourell, J. Beaman, H. Marcus, Direct selective laser sintering of metals, Rapid Prototyp. J. 1 (1995) 26-36.

[6] N. Guo, M. C. Leu, Additive manufacturing: technology, applications and research needs, Front. Mech. Eng. 8 (2013) 215-243.

[7] Z. Weng, J. Wang, T. Senthil, L. Wu, Mechanical and thermal properties of ABS/montmorillonite nanocomposites for fused deposition modelling 3D printing, Mater. Design, 102 (2016) 276-283.

[8] S. Ambriz, J. Coronel, B. Zinniel, R. Schloesser, C. Kim, M. Perez, C. Espalimn, R.B. Wicker, Material handling and registration for an additive manufacturing-based hybrid system, J. Manufacturing Sys. 45(2017) 17-27.

[9] E. MacDonald, R. Wicker, Multiprocess 3D printing for increasing component functionality, J. Sci. 353 (2016) 1-8.

[10] J.L. Coronel Jr., K.H. Fehr, D.D. Kelly, D. Espalin, R.B. Wicker, Increasing component functionality via multi-process additive manufacturing, Proc. of SPIE 10194 (2017) 101941F-1-101941F-8.

[11] A.J. Lopes, M. Navarrete, F. Medina, J. Palmer, E. MacDonald, R.B. Wicker, Expanding rapid prototyping for electronic systems integration of arbitrary form, in Proceedings. 17th Annual International Solid Freeform Fabrication Symposium, (2006).

[12] F. Medina, A.J. Lopes, A.V. Inamdar, R. Hennessey, J.A. Palmer, B.D. Chavez, R.B. Wicker, Integrating multiple rapid manufacturing technologies for developing advanced customized functional devices, in Proceedings. Rapid Prototyping & Manufacturing 2005, (2005) 10-12.

[13] F. Medina, A.J. Lopes, A.V. Inamdar, R. Hennessey, J.A. Palmer, B.D. Chavez, D. Davis, P. Gallegos, R.B. Wicker, Hybrid manufacturing: integrating stereolithography and direct write technologies, in Proceedings. 16th Annual International Solid Freeform Fabrication Symposium, (2005) 39-49.

[14] E. Malone, H. Lipson, Freeform fabrication of ionomeric polymer-metal composite actuators, Rapid Prototyp. J. 12 (2006) 244-253.

[15] E. Malone, M. Berry, H. Lipson, Freeform fabrication and characterization of Zn-air batteries, Rapid Prototyp. J. 14 (2008) 128-140.

[16] D. Periard, E. Malone, H. Lipson, Printing embedded circuits, in Proceedings. 18th Annual International Solid Freeform Fabrication Symposium, (2007) 503-512.

[17] J. DeGrange, B. Macy, Smart parts: additive manufacturing for integrated electro-mechanical devices, Webinar. Available: https://www.designworldonline.com/category/webinars (26 June 2019).

[18] J.A. Paulsen, M. Renn, K. Christenson, R. Plourde, Printing conformal electronics on 3D structures with Aerosol Jet technology. Future of Instrumentation International Workshop, in Proceedings. (2012) 1-4.

[19] https://www.optomec.com/wp-content/uploads/2014/04/AJ_Printed_Electronics_Overview_whitepaper.pdf (25 June 2019).

[20] J.A. Lewis, B.Y. Ahn, Device fabrication: three-dimensional printed electronics, Nature 518 (2015) 42-43.

[21] https://support.voxel8.co/hc/en-us/articles/207469773-Developer-s-Kit-Platform-Overview (25 June 2019).

[22] https://www.nano-di.com/ (25 June 2019).

[23] C.M. Shemelya, M. Zemba, C. Kief, D. Espalin, R.B. Wicker, E. MacDonald, Multi-layer off-axis patch antennas fabricated using polymer extrusion 3D printing. Proceedings of the European Conference on Antennas and Propagation (2016).

[24] A.D. Valentine, T.A. Busbee, J.W. Boley, J.R. Raney, A. Chortos, A. Kotikian, J.D. Berrigan, M.F. Durstock, J.A. Lewis, Hybrid 3D printing of soft electronics, Adv. Mater. 29 (2017) 1703817.

[25] D. Espalin, D.W. Muse, E. MacDonald, R.B. Wicker, 3D printing multifunctionality: structures with electronics, Int. J. Adv. Manuf. Technol. 72 (2014) 963-978.

[26] E. MacDonald, D. Espalin, D. Doyle, J. Munoz, S. Ambriz, J. Coronel, A. Williams, R. Wicker, Fabricating patch antennas within complex dielectric structures through multi-process 3D printing, J. Manuf. Process. 34 (2018) 197-203.

[27] X. Wang, J. Liu, Recent advancements in liquid metal flexible printed electronics: properties, technologies, and applications, Micromachines 7 (2016) 206.

[28] B.Y. Ahn, S.B. Walker, S.C. Slimmer, A. Russo, A. Gupta, S. Kranz, E.B. Duoss, T.F. Malkowski, J.A. Lewis, Planar and three-dimensional printing of conductive inks, J. Visual. Exp. 58 (2011) e3189.

[29] W. Wu, Inorganic nanomaterials for printed electronics: a review, Nanoscale 9 (2017) 7342-7372.

[30] A. Kamyshny, S. Magdassi, Conductive nanomaterials for 2D and 3D printed flexible electronics, Chem. Soc. Rev. 48 (2019) 1712-1740.

[31] https://www.printedelectronics.com/printed/materials/ (25 June 2019).